International Academic Institute for Science and Technology

International Academic Journal of Science and Engineering
Vol. 3, No. 2, 2016, pp. 55-70.
ISSN 2454-3896

International Academic Journal of Science and Engineering

www.iaiest.com

Pressure Losses Analysis in Air Duct Flow Using Computational Fluid Dynamics (CFD)

Ikpe Aniekan Essienubong[a], Ejiroghene Kelly Orhorhoro[b*]

[a] *Mechanical Engineering Department Coventry University, UK,.*

[b] *Cemek Machinery Company, Benincity, Nigeria.*

Abstract

In this paper, hand calculation and computer simulation was used to determine the pressure loses in air duct flow system for velocity of 5m/s, 10m/s, 20m/s and 40m/s and the results were compared to determine their accuracies. Total maximum pressure was recorded at inlet, while least pressure was observed at outlet. The pressure losses for both hand, and computer simulation increased proportionally to the velocity. Also, both pressures lose obtained from the hand calculation and simulation almost maintained the same pattern and direction. But for purpose of accuracy and fast computation, simulation is preferable.

Keywords: Pressure losses, Air duct flow, Velocity, Simulation

Introduction:

Fluid flow in circular and noncircular pipes is commonly encountered in our industry on a daily basis ranging from the oil industry, brewery industry, power sector, institution etc. (Barati, 2012). Also natural gas is transported hundreds of miles through large pipelines. It can equally be applied in a car engine, cool water is transported by hoses to the pipes in the radiator where cooling is done as it flows. However, for proper installation of air distribution systems, the type of duct fittings used plays major role in the overall system performance (Abushakra, et al., 2002). It is vital for the designer engineer to put into consideration the impact of pressure drop in flexible ducts. Pressure loss is as result of pressure drop and is due to the difference in pressure in between two points in a flow system (IBACOS, 1995). It arises from frictional force caused by resistance to flow, and it acts on the fluid as flow progresses across the channel such as duct which could be internal or external (Walker, et al., 2001). The major factor that determines resistance to fluid flow includes fluid viscosity and velocity. This is because pressure difference due to pressure drop increases directly proportional to the frictional shear force within the duct network (Kokayko, et al., 1996). Moreover, a flow system with high flow velocity or high flow viscosity may result in a large pressure difference across the section of the duct, especially at the bends (ACCA, 1995). Fluid flow can be classified as either external or internal, depending on whether the required fluid is forced to flow over a surface or simply in a conduit. In this research paper, the flow is internal, and is driven primarily by a pressure difference. Also, a CFD package-Star CCM+ was used to analyze pressure losses in air duct flow. The K-epsilon turbulence model was applied in the simulation, and it is one of the common turbulence models used by Star CCM+ in resolving turbulent flow. This model is recommended for use for flows that do not involve heat transfer (Cengel, et al., 2012; Adapco, 2013). The letter "k" is the turbulent kinetic energy while ε is the rate of dispersion of the turbulent energy. K- Epsilon model resolves turbulence by finding the amount of kinetic energy per unit mass present in the turbulent fluctuations (Barati 2012; Scott-Pomerantz 2004).

Research methodology

As discussed earlier in the introductory part of this paper, pressure loss plays a vital role in fluid mechanics, the higher the pressure, the high the flow of fluid in a given duct. This implies that it is important to determine the pressure of a material such as liquid or gas in a given duct, for proper design and installation of the flow system. In this paper, hand calculation and computer simulation was used to determine the pressure loses in air duct flow system for velocity of 5m/s, 10m/s, 20m/s and 40m/s and the results were compared to determine their accuracies.

Hand Calculations for Pressure Losses

For flow within pipes, there will be pressure loss over the pipe length due to friction and pressure loss due to bends.

Therefore;

$$h_l = h_{lpipe} + h_{lbends} \quad (1)$$

This is because the geometry of the pipe is constant throughout the flow as shown in Figure (1). There are two bends of 90 degrees each in the pipe geometry.

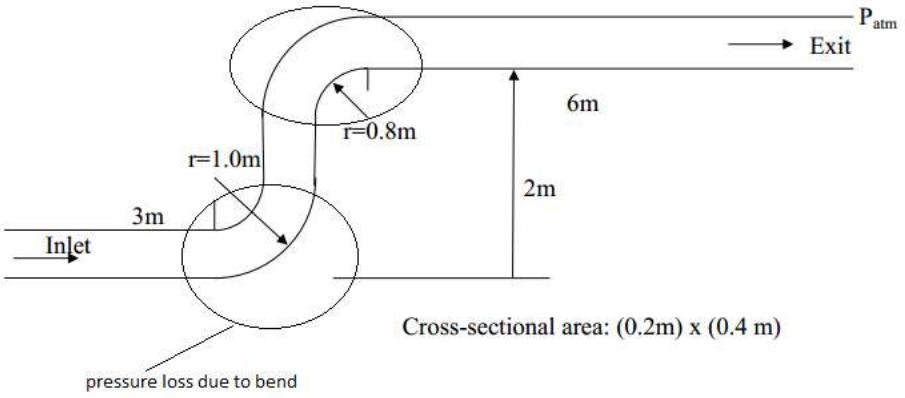


Figure 1. Pressure losses in air duct flow

Pressure Losses over the Pipe Length

Pressure loss in pipes is given as;

$$h_{lpipe} = f(R_e) \times \left(\frac{L}{D}\right) \times \frac{v^2}{2g} \tag{2}$$

Where:

$$f = \frac{0.25}{\left[Log\left(\frac{\varepsilon}{3.7D} + \frac{5.74}{R_e^{0.9}}\right)\right]^2} \tag{3}$$

L is the length of the pipe in meters
D is the diameter of the pipe in meters
V is the velocity of the flow through the pipe
R_e is the Reynolds number and is given as
ε: Surface Roughness (0.0025 x 10^{-3}m)

For $v = 5ms^{-1},\ R_e = 89000\ and\ D_h = L = 0.267m$

$$f(Re) = \frac{0.25}{\left[\log\left(\left(\frac{\varepsilon}{3.7d}\right) + \left(\frac{5.74}{Re^{0.9}}\right)\right)\right]^2} \tag{4}$$

$$= \frac{0.25}{\left[\log\left(\left(\frac{0.0025\times10^{-3}}{3.7\times0.267}\right) + \left(\frac{5.74}{89000^{0.9}}\right)\right)\right]^2}$$

$$= \frac{0.25}{[\log(2.5306\times10^{-6} + 2.0159\times10^{-4})]^2}$$

$$= \frac{0.25}{[\log 0.000204120 6]^2}$$

$$= \frac{0.25}{[-3.6901]^2} = \frac{0.25}{13.6169}$$

$$f(Re) = 0.01836$$

The total effective length of the pipe is 9.2m

That is,

$$v = 5ms^{-1}, D_h = 0.267m, \ and \ L = 9.2m$$

$$h_{lpipe} = f(R_e) \times \left(\frac{L}{D}\right) \times \frac{v^2}{2g} \quad (5)$$

$$= \frac{0.01836 \times 9.2 \times 5^2}{0.267 \times 2 \times 9.81} = 0.8061m$$

The major head loss is 0.8061m

For other velocities, Table 1 shows the values for the friction factor and the major head loss.

Table 1: Values of friction factor and the major head loss for different velocities

Velocity (m/s)	Reynolds number	$f(R_e)$	h_{lpipe}
5	89000	0.01836	0.8061
10	178000	0.01597	2.8047
20	356000	0.01405	9.8699
40	712000	0.01249	35.0962

Pressure losses due to bends

As shown in Figure 2, the two minor losses due to the 90^0 bends can be estimated by:

$$h_{lbends} = k_l \times \frac{v^2}{2g} \quad (6)$$

Where:

k_l: is the frictional factor due to flow across bends and is given 1.1 for 90^0 bends without vanes.

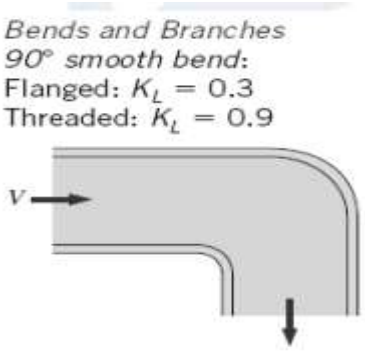


Figure 2. k_l value for pipe bends (Cengel et al., 2012)

$$h_{lbend} = 2\left(0.3 \times \frac{5^2}{2\times 9.81}\right) = 0.7645m$$

For other velocities, Table 2 shows the values for the bend friction factor and the minor head loss, while Table 3 represents summary of total pressure loss head in the pipe for different velocities. Furthermore, Table 4 presents summary of total pressure loss, Pressure loss smooth and pressure loss coarse.

Table 2 Values of bend friction factor and the minor head loss for different velocities

Velocity (m/s)	Reynolds number	k_l	h_{lbends}
5	89000	0.3	0.7645
10	178000	0.3	3.0581
20	356000	0.3	12.2324
40	712000	0.3	48.9296

Summarily,

Table 3. Summary of total pressure loss head in the pipe for different velocities

Velocity (m/s)	Reynolds number	h_{lpipe}	h_{lbends}	Total Pressure Loss
5	89000	0.8061	0.7645	1.5706
10	178000	2.8047	3.0581	5.8628
20	356000	9.8699	12.2324	22.1023
40	712000	35.0962	48.9296	84.0258

The Energy equation for pipes can be given as

$$\Delta P = \rho g h_{losses} \quad (7)$$

For smooth pipe the losses will only include the losses at the bend

That is,

For 5m/s,

$$\Delta P = \rho g h_{losses} = 1.2 \times 9.81 \times 0.7645 = 9.00Pa$$

For rough pipes, the losses will include the losses at the bend

That is,
For 5m/s,
$$\Delta P = \rho g h_{pressure\ losses} = 1.2 \times 9.81 \times 1.5706 = 18.49Pa$$

Table 4. Summary of total pressure loss, Pressure loss smooth and pressure loss coarse

Velocity (m/s)	h_{lbends}	Total Pressure Loss	Pressure Loss Smooth	Pressure Loss Coarse
5	0.7645	1.5706	9.00	18.49
10	3.0581	5.8628	36.00	69.02
20	12.2324	22.1023	144.00	260.19
40	48.9296	84.0258	576.00	989.15

STAR CCM Modelling/Simulation

The various steps taken in the star CCM simulation of the flow analyses is shown below.

Cad Model

The first step in the modelling is to create the geometry of the duct either in STARCCM+ or any other CAD software. For this report, the model was created in CATIA. The CATIA representation is shown in Figure 3. The CATIA model was then saved in a format that was compatible with the STARCCM+ software.

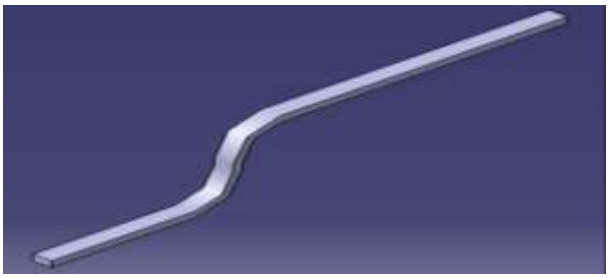


Figure 3. Representation of the air flow duct

Model Import

With the STAR CCM+ interface opened, a new simulation in started with the power on demand license and the parallel on local host process option. The CATIA file was then imported into the model as a region. The one boundary per face option was used; one region per body and the sewing tolerance was 0.001 as shown in Figure 4, while the STAR-CCM+ Imported model is shown in Figure 5.

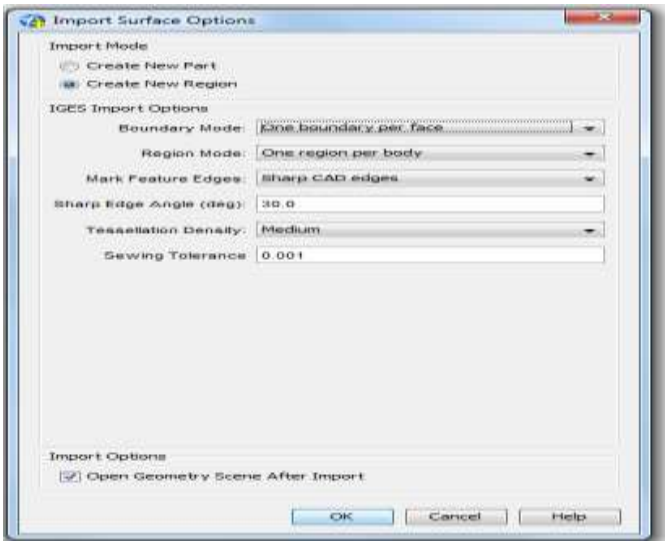


Figure 4. Import tool box from CATIA to STAR CCM+



Figure 5. STAR-CCM+ Imported view of the air duct

Model Mesh

The generated regions were divided into three: the input, Output and the Wall. The input was assigned velocity inlet type, and the output was assigned pressure outlet type. The regions were then prepared for mesh in the continua by choosing the surface mesher, the polyhedral mesher and the prism layer mesher as shown in Figure 6.

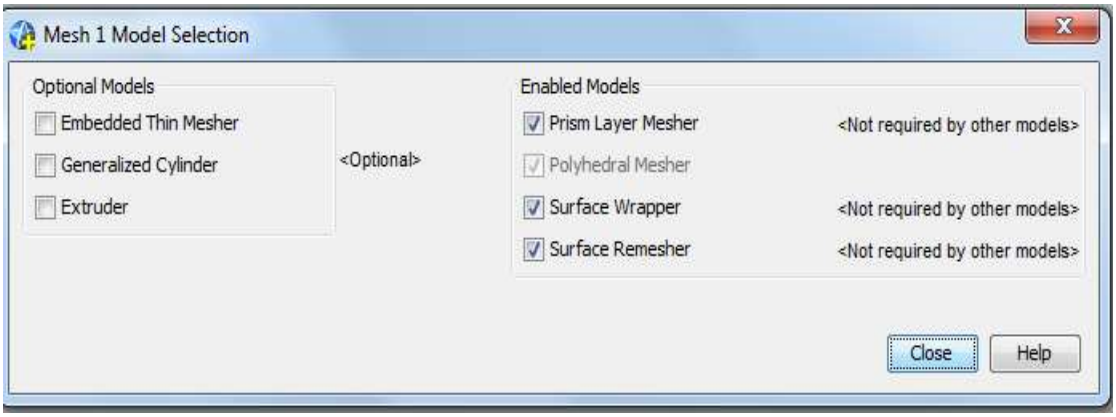


Figure 6. Meshing tool box for the airflow duct

A mesh is regarded as the discretized representation of a model otherwise termed the computational domain. This domain is utilized by the solver to produce a numerical solution of the scenario being modelled. The meshing follows the part-based meshing principle in STAR-CCM+. The surface remesher obtains a high-quality surface mesh by re-triangulating closed surfaces. In order to improve the overall quality of an existing surface and optimize it for the volume mesh models, the surface remesher can be used to retriangulate the surface. The remeshing is primarily based on a target edge length that you supply and can also include feature refinement that is based on curvature and surface proximity. Localized refinement that is based on part surfaces or boundaries can also be included. Polyhedral meshes provide a balanced solution for complex mesh generation problems. They are relatively easy and efficient to build, requiring no more surface preparation than the equivalent tetrahedral mesh. They also contain approximately five times fewer cells than a tetrahedral mesh for a given starting surface. Multi-region meshes with a conformal mesh interface are allowed. The prism layer mesh model is used with a core volume mesh to generate orthogonal prismatic cells next to wall surfaces or boundaries. This layer of cells is necessary to improve the accuracy of the flow solution (C D Adapco, 2013). A 3D mesh of the duct was processed using polyhedral mesher with prism layer equivalent to the boundary layer thickness calculated and as displayed in table 10. The 3D mesh was however converted to 2D to enhance the processing time for the analysis. The 3D and 2D mesh of the duct is shown in Figures 7 respectively.

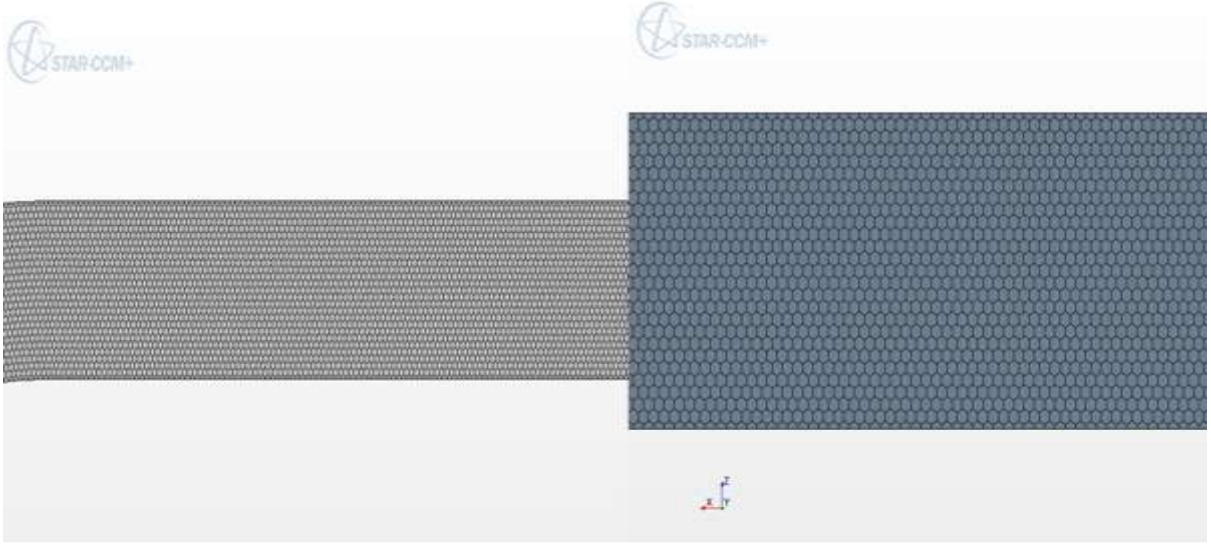


Figure 7. 2D and 3D Mesh of the Duct

Mesh Convergence Study

To ensure adequate compensation between accuracy and CPU run time, the analysis of the maximum velocity in the subsystem was done to evaluate the result of each mesh size and subsequently determine the best mesh size for the flow. Generally the number of cell generated increases with reduced mesh size and vice versa. Increased accuracy is achieved with higher number of cells but there is a geometric increase in computing time. Generally, as the number of cells is increased, the results obtained become more accurate while the computational time increases also. The point where the mesh size contributes lesser to change in the results is the required value of the mesh. However as the mesh size is made finer and the number of cells increased, a point is reached when the results obtained is not marginally affected by the mesh size. At this point the mesh size is said to have converged. From Figure 8, the best mesh size will therefore be 8mm

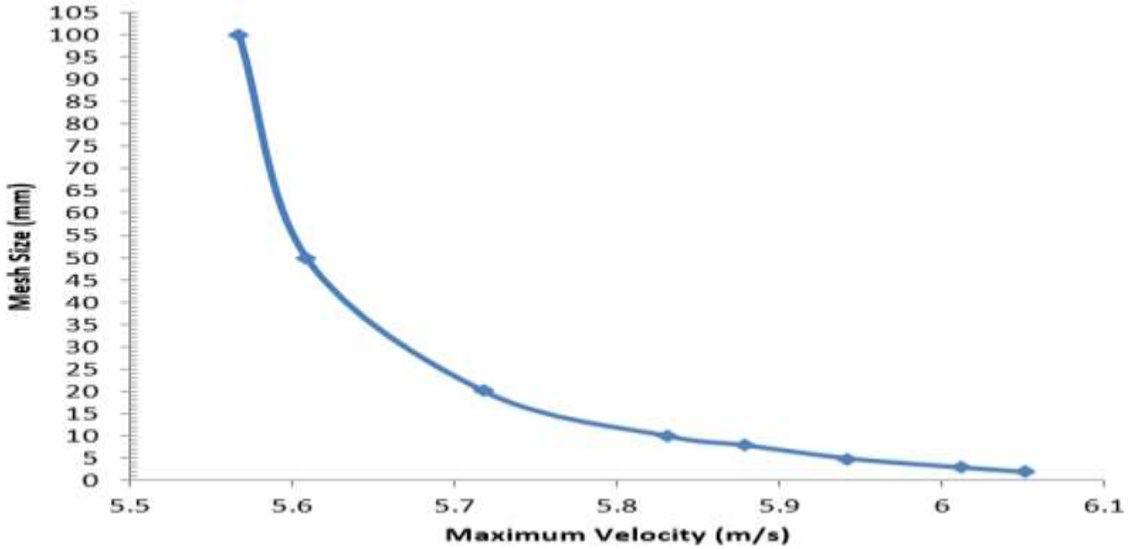


Figure 8. Mesh Convergence Study

Model Physics

The fluid simulated in the analysis is a real fluid. It is therefore expected that there will be build-up of viscous forces along the walls that will resist the fluid flow. This phenomenon will result in zero velocities along the walls of the duct. This condition is called a "No slip condition" and is a characteristic of real fluids. It is however worthy to note that the average velocity throughout the flow will remain the same. The duct is assumed to be stationary for the duration of the flow. The temperature of the system is also expected to remain the same. This however means that there will be variation in the volume of air across the duct. The fluid density is also expected to remain constant. A summary of the physics for the flow simulation in STAR CCM+ is shown in Table 5.

Table 5. Summary of the Model Physic for simulation

Parameters	**Functional Requirement**	**Selection/ Value Inputted**
Mesh Selection	Mesh type	Polyhedral (for Volume Mesh) Surface Remesher (Surface mesh) Prism Layer Mesh (For the prism layer)
	Base size	8mm
	Prism Layer thickness	0.05228
	Number of layers	6
	Prism layer stretching	1.5
Physics Selection	Space	2D flow
	Time	Steady
	Material	Gas
	Flow	Segregated flow
	Equation of State	Constant density
	Viscous Regime	Turbulent
	Reynolds-Averaged Turbulence	K-epsilon
Boundary condition selection	Inlet	Inlet Velocity
	Outlet	Outlet Pressure
	Wall	Wall
	Turbulent Intensity	Calculated values
	Turbulence Specification	Intensity + Length scale
	Turbulent length scale	7% of the Hydraulic diameter
	Turbulent velocity scale	10% of the free steam velocity
	Temperature	293K
	Wall condition	No-slip

Considering the 2D simulation for the analysis was necessary because of the run time for the simulation. Since a material for the pipe was not given the walls of the pipe was assumed to be smooth. This therefore implies that the pressure drop calculator will omit the pressure loss due to the pipe length during calculation. The various physical and many other material properties of the flow at different temperatures are given as show on Table 6.

Table 6. Summary of Physical condition of the flow at different velocities

Velocity (m/s)	Reynolds number	Mach number	Mass flow rate kg/s	Turbulence Intensity	Turbulence Length Scale	Reynolds number Re_x	Boundary layer thickness (m)
5	89000	0.0146	0.48	0.03850	0.01869	667000	0.05228
10	178000	0.0292	0.96	0.03530	0.01869	1333000	0.04551
20	356000	0.0584	1.92	0.03237	0.01869	2667000	0.03962
40	712000	0.1168	3.84	0.02969	0.01869	5333000	0.03449

Total Pressure

A plot of the total pressure shows the pressure gradient across the whole pipe for each run of velocity. Figures 9 to 12 show the total pressure plot for each velocity of the simulation.

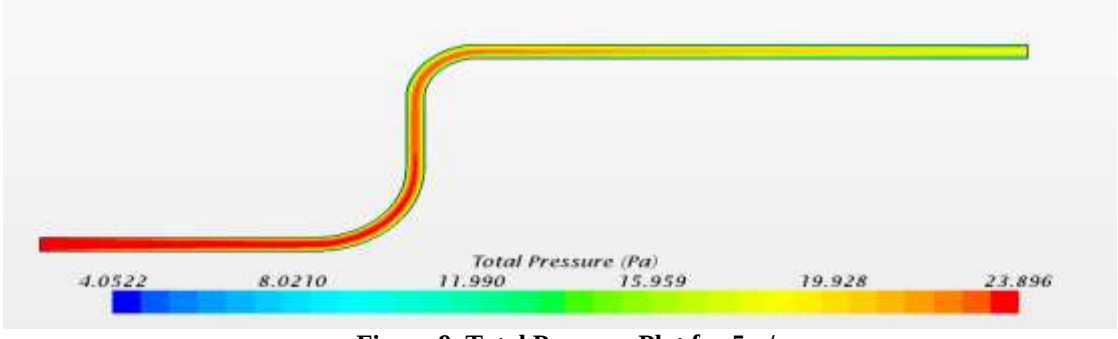


Figure 9. Total Pressure Plot for 5m/s

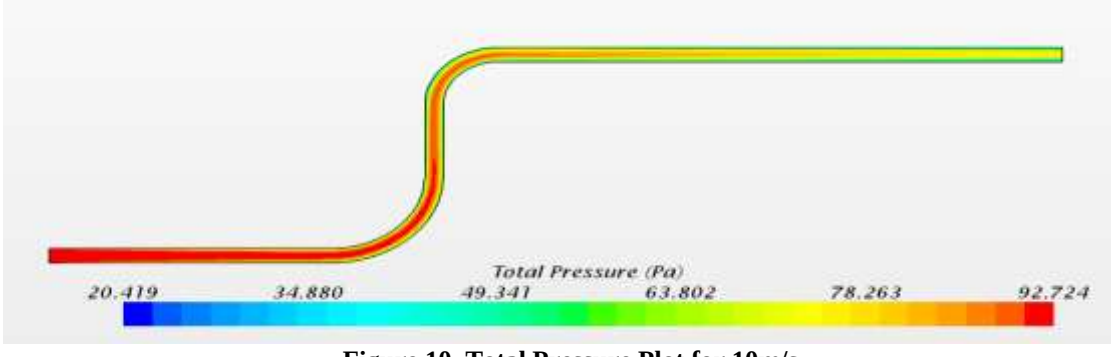


Figure 10. Total Pressure Plot for 10m/s

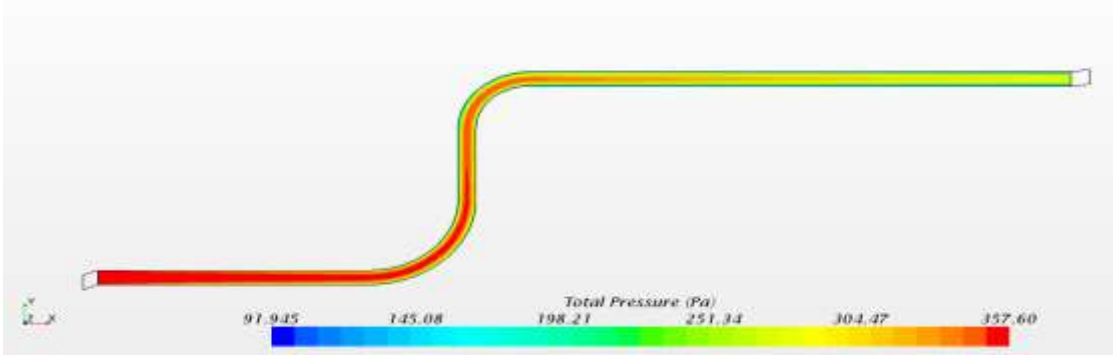


Figure 11. Total Pressure Plot for 20m/s

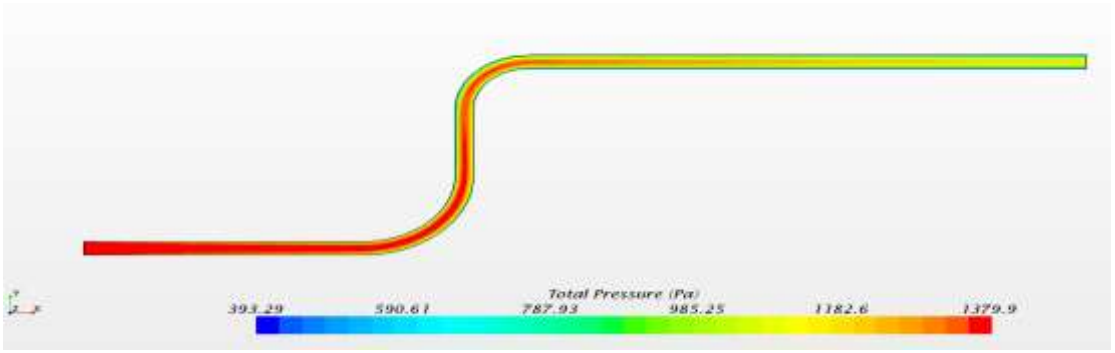


Figure 12. Total Pressure Plot for 40m/s

As the velocity increases, the total pressure at the inlet and the outlet increases. An obvious boundary layer is observed in the flow at a distance from the entrance showing that there is an obvious reaction between the walls of the duct and the air flowing through the system. The total pressure is maximum at the inlet and least in the outlet. This phenomenal pressure gradient in the duct ensures that the fluid is transported with minimum work done.

Pressure Drop

The estimated pressure losses from the simulation for each velocity are given in Table 7, while Table 8 shows summary of Pressure drop from hand calculations and simulation. The plot of pressure drop against velocity for hand calculations and simulation is shown in Figure 13.

Table 7. Estimated pressure losses from the simulation for each velocity

Pressure drop Plot for 5m/s
Difference of Total Pressure: Inlet/Outlet --- Total Pressure Drop: 7.647930e+00 (Pa)
Pressure drop Plot for 10m/s
Difference of Total Pressure: Inlet/Outlet --- Total Pressure Drop: 2.852772e+01 (Pa)
Pressure drop Plot for 20m/s
Difference of Total Pressure: Inlet/Outlet --- Total Pressure Drop: 1.032651e+02 (Pa)
Pressure drop Plot for 40m/s
Difference of Total Pressure: Inlet/Outlet --- Total Pressure Drop: 3.691731e+02 (Pa)

Table 8. Summary of Pressure drop from hand calculations and simulation

Velocity (m/s)	Pressure Loss Smooth	Pressure Loss Coarse	Computation	% Error smooth	% Error coarse
5	9.00	18.49	7.65	15.00	58.63
10	36.00	69.02	28.53	20.75	58.66
20	144.00	260.19	103.27	28.28	60.31
40	576.00	989.15	369.17	35.91	62.68

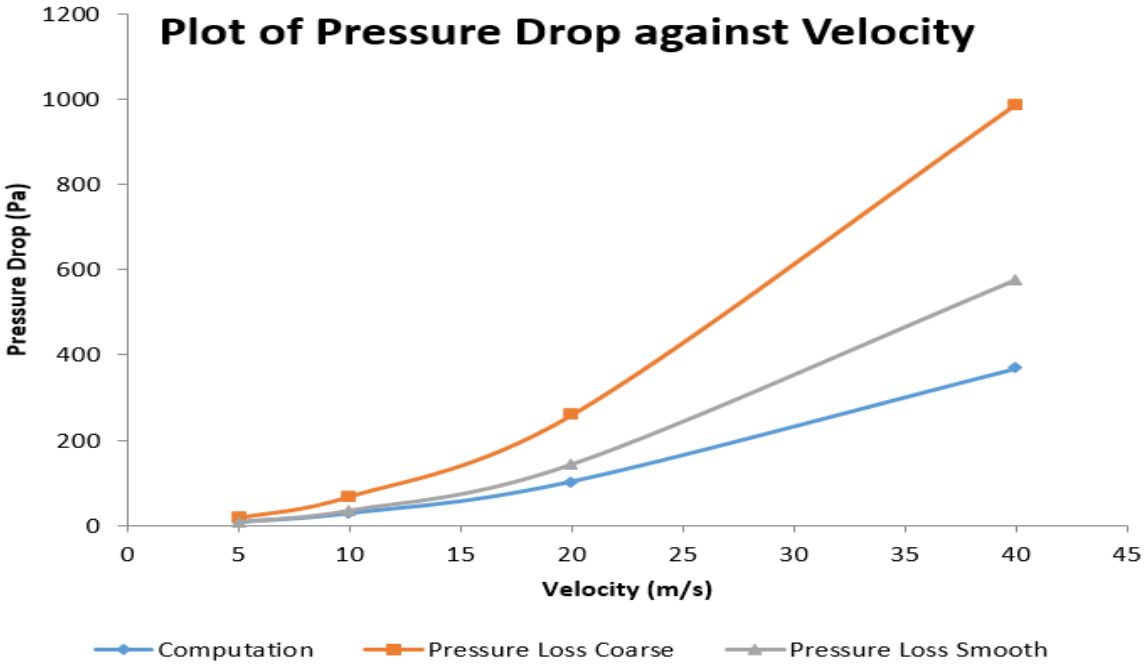


Figure 13. Plot of Pressure drop against velocity for hand calculations and simulation

Conclusion

From Table 8, using 1D formula to calculate pressure drop for pipe when it is coarse or smooth showed that the smooth pipe assumptions gave a somewhat closer value to the results from the computation. This is possible because the simulation was 2D and the calculations were 1D formula for pressure loss in pipes. For velocity of 5m/s, 10m/s, 20m/s and 40m/s used in this paper, it can be observed that the pressure losses increased as the velocity increased, and from Figure 13, both pressure loses obtained from the hand calculation and pressure losses obtained from the simulation almost maintained the same pattern and direction. Hence, the pressure losses can be calculated using hand calculation and through simulation, but for the purpose of achieving minimal errors and less time, simulation method is most preferred as normally applied in industries. From the graph shown in Figure 13, it can be concluded that the disparity between the hand calculations is due to approximation of the k-epsilon model used by the solver to interpret the flow.

References

Abushakra, B., Dickerhoff, D., Walker, I. and Sherman M. (2002). Laboratory Study of Pressure Losses in Residential Air Distribution Systems. Lawrence Berkeley National Laboratory Report LBNL-49293, Berkeley, CA (in press).

ACCA. (1995). Residential Duct Systems. Manual D. Air Conditioning Contractors of America. Washington, DC.

Adapco, C.D. (2013). User guide: STAR-CCM+ Version 8.04 [online] available from <http://cumoodle.coventry.ac.uk/course/view.php?id=15595> [2 March 2014]

Barati, R. (2012). Numerical Investigation of Turbulent Flows Using k-epsilon [online] available

Bench Tests. IBACOS – Burt Hill Project 95006.13.Pittsburgh, PA.

Cengel, Y., CIMBALA, J., TURNER, R., and KANOGLU, M. (2012). Thermo-FluidSciences. Newyork:

from<https://www.google.co.uk/url?sa=t&rct=j&q=&esrc=s&source=web&cd=10&cad=rja&uact=8&ved=0CHwQFjAJ&url=http%3A%2F%2Fwww.researchgate.net%2Fprofile%2FReza_Barati%2Fpublication%2F235407247_Numerical_simulation_of_turbulent_flows_using_k-epsilon%2Ffile%2F9fcfd5114c8f0aad54.ppt&ei=wt1WU4KiAsiv7AbK2YCoDA&usg=AFQjCNHoUARNQkkAvUljUIGkDtZ1g8-2cg&bvm=bv.65177938,d.ZGU> [24 March 2014]

IBACOS (1995). Ventilation Ducts and Registers – Interim Milestone Report. IBACOS, Pittsburgh, PA.

Kokayko, M., Holton, J., Beggs, T., Walthour, S., and Dickson, B. 1996. Residential Ductwork and Plenum Box

MgGraw-Hill.

Scott-Pomerantz, C. (2004). The k-epsilon Model in the theory of Turbulence [online] available from <http://d-scholarship.pitt.edu/10241/1/cdsp-new.pdf > [24 April 2014]

Walker, I.S., Wray, C.P., Dickerhoff, D.J., and Sherman, M.H. (200). Evaluation of Flow Hood Measurements for Residential Register Flows. LBNL 47382.